Available online at www.sciencedirect.com
SCIENCE DIRECT®
Journal of Solid State Chemistry 178 (2005) 382–389
JOURNAL OF SOLID STATE CHEMISTRY
www.elsevier.com/locate/jssc

Rapid communication

Combustion synthesis of Ni–Zn ferrite powder—influence of oxygen balance value

Chyi-Ching Hwang[a,*], Jih-Sheng Tsai[a], Ting-Han Huang[a], Cheng-Hsiung Peng[b], San-Yuan Chen[b]

[a]*Department of Applied Chemistry, Chung Cheng Institute of Technology, National Defence University, Number 190, Sanyuan First Street, Tashi Jen, Taoyuan 33509, Taiwan*

[b]*Department of Materials Science and Engineering, National Chao Tung University, Hsinchu 300, Taiwan*

Received 30 August 2004; received in revised form 26 October 2004; accepted 28 October 2004

Abstract

In this study, $Ni_{0.5}Zn_{0.5}Fe_2O_4$ powder was synthesized via an exothermic reaction between nitrates [$Ni(NO_3)_2 \cdot 6H_2O$, $Zn(NO_3)_2 \cdot 6H_2O$, $Fe(NO_3)_3 \cdot 9H_2O$, and NH_4NO_3] and glycine [NH_2CH_2COOH]. By adjusting the glycine-to-nitrates ratio, the oxygen balance (OB) values of the reactant mixtures can be varied in which the combustion phenomena is altered and thereby the as-synthesized products with different characteristics are obtained. An interpretation based on the measurement of maximum combustion temperature (T_c) and the amounts of gas evolved during reaction for various OB values has been proposed regarding the nature of combustion and its correlation with the characteristics of as-synthesized products. After instrumental analyses, it is shown that the as-synthesized powders are nanoscale crystallites with a large specific surface area and they inherit a superparamagnetic behavior.

Keywords: Combustion synthesis; Nanocrystalline; Oxygen balance; Nitrates; Glycine

1. Introduction

In the past decade, a solution combustion method has been narrated and utilized to synthesize simple and mixed metal oxides [1–9]. With this method, the heating and evaporation of desired nitrate solution employing an organic compound (usually glycine, urea, or citric acid, etc.) can result in self-firing to generate heat by exothermic reaction. This liberated heat is used to synthesize the ceramic oxide powders. Together, this method has advantages of applying inexpensive raw materials, maintaining a relatively simple, quick and straightforward preparation process, and achieving a fine powder with high homogeneity. Recently, a wide range of technological applications has made homogeneous and nano-crystalline particles the necessary materials in electronics industry. Ni–Zn ferrite with its commercial usage in power transformers, microwave devices and telecommunication applications [10] made a favorable choice due to its high resistivity, low coercivity and inappreciable eddy current loss [11] arising from the fact that they are capable of being used as a soft-magnetic material.

In this study, to open the door to sources of other preferences, $Ni_{0.5}Zn_{0.5}Fe_2O_4$ was synthesized using metal (Ni, Zn, Fe) nitrates (acting as the dual roles of oxidant and metal source), ammonium nitrate (oxidant) and glycine (fuel) via combustion reaction. Glycine was chosen as fuel owing to its inexpensive price. Also, its melting point is higher and its heat of combustion is more negative when compared with urea and citric acid. When complete combustion is assumed, the reaction equation can be expressed (greatly

*Corresponding author. Fax: +886 3 389 2494.
E-mail address: cchwang1@ccit.edu.tw (C.-C. Hwang).

0022-4596/$ - see front matter © 2004 Elsevier Inc. All rights reserved.
doi:10.1016/j.jssc.2004.10.045

simplified) as follows:

$$0.5Ni(NO_3)_2 \cdot 6H_2O_{(c)} + 0.5Zn(NO_3)_2 \cdot 6H_2O_{(c)} + 2Fe(NO_3)_3 \cdot 9H_2O_{(c)} + \psi NH_2CH_2COOH_{(c)} + \kappa NH_4NO_{3(c)} \xrightarrow{\text{mixing \& dehydration}} Ni_{0.5}Zn_{0.5}Fe_2C_{2\psi}H_{5\psi+4\kappa}N_{8+\psi+2\kappa}O_{24+2\psi+3\kappa}$$

(the general formula of mixture) $\xrightarrow{\text{combustion}}$

$$Ni_{0.5}Zn_{0.5}Fe_2O_{4(c)} + 2\psi CO_{2(g)} + \left(\frac{5\psi}{2} + 2\kappa\right)H_2O_{(g)} + \left(4 + \frac{\psi}{2} + \kappa\right)N_{2(g)} + \left(10 - \frac{9\psi}{4} + \frac{\kappa}{2}\right)O_{2(g)} \left(\left(14 + \frac{11}{4}\psi + \frac{7}{2}\kappa\right)\text{moles of gas produced}\right). \quad (1)$$

According to the definition of oxygen balance (OB) employed in the field of propellants and explosives described in Ref. [12], it is appropriate to express OB value in terms of the weight percent of excessive oxygen required versus the formula weight of the mixture.

$$OB(\%) = \frac{AW_{oxygen}}{FW_{mixture}}\left(20 - \frac{9\psi}{2} + \kappa\right) \times 100\%, \quad (2)$$

where AW_{oxygen} and $FW_{mixture}$ are the atomic weight of oxygen and the formula weight of the mixture, respectively. From Eqs. (1) and (2), OB value of the reactant mixture can be adjusted by varying the values of Ψ and κ, as illustrated below:

1. OB < 0 (fuel-rich), when $\Psi > \frac{40}{9}(\cong 4.44)$ and $\kappa = 0$. Obtaining oxygen from atmosphere is required for combustion between glycine and metal nitrates.
2. OB = 0 (stoichiometric), when $\Psi = 4.44$ and $\kappa = 0$. The oxygen content of metal nitrates can react completely in oxidizing glycine equivalently.
3. OB > 0 (fuel-lean), when $\Psi = 4.44$ and $\kappa > 0$. There is an excess amount of oxygen in the reactant mixture caused by the addition of NH_4NO_3.

Although there exist some literatures reporting that nano-sized Ni–Zn ferrites were synthesized by the combustion method [4,8,9,11,13–16], hardly is any information available on the effects of reactant composition (i.e., the OB value), the nature of combustion reaction, and the properties of as-synthesized powders. In this work, the study of correlation among the OB value, reaction phenomena and product characteristics are undertaken.

2. Experimental

2.1. Sample synthesis

$Ni_{0.5}Zn_{0.5}Fe_2O_4$ powder was synthesized by an amount of 25 g per batch. After considering both economy and accuracy of the experiment, the OB value was limited in the region of −15%–+10%. At a desired OB value, the starting materials $Ni(NO_3)_2 \cdot 6H_2O$, $Zn(NO_3)_2 \cdot 6H_2O$, and $Fe(NO_3)_3 \cdot 9H_2O$ (all ⩾99.0%, Merck, Germany) and glycine and NH_4NO_3 (both ⩾98.0%, Riedel-de Haën, Germany) were directly mixed in a porcelain crucible without adding water, resulting in a slurry substance due to the hygroscopicity of nitrates. (It is our finding to omit the procedure of dissolving the reactants in water to form a solution). This reactant mixture was heated by using a hot-plate at ~100 °C to a state of dehydration. In the meantime, the reactant mixture was stirred vigorously by using a magnetic agitator to homogenize, in that the dried reactant mixture was ignited to start combustion reaction by using mini gas burner in air at room temperature. In Fig. 1, the combustion reaction of the dried reactant mixture is illustrated in the case of OB= 0.

2.2. Characterization

Pt/Pt–10%Rh thermocouple of diameter 0.127 mm was used to measure the temperature variations during combustion reaction and an alumina tube of 1.2 mm was inserted into the reactant mixture to reduce the measuring disturbance resulting from the violent gas evolution occurred during reaction. Concurrently, the signals from the thermocouple were stored and processed using a data acquisition system (NOTEBOOK, Labtech, Wilmington, MA). Phase formation of the product was identified by X-ray diffraction (XRD; SIEMENS D5000) with Cu$K\alpha$ radiation ($\lambda = 1.5418$ Å). The morphological feature of the

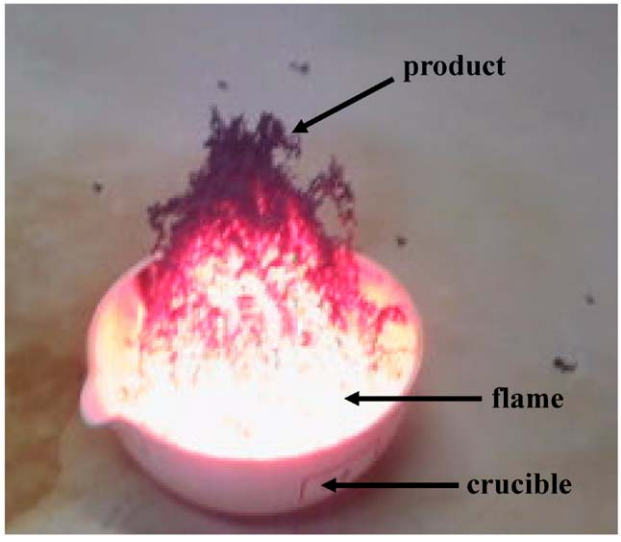

Fig. 1. Combustion reaction of dried reactant mixture with OB= 0. Luminous flame and smoke gas arise as the dried reactant mixture is ignited, causing the product left behind to be dry and fluffy in nature.

product powder can be observed by a scanning electronic microscope (SEM; Hitachi S-3000N) with an accelerating voltage of 15 kV. The grain size and the electron diffraction pattern of the product were imaged by transmission electron microscope (TEM; Hitachi H-7100). As far as TEM studies are concerned, as-synthesized products were fully grounded and treated with oscillation thoroughly, then the powders were supported on carbon-coated copper TEM grids and analyzed at an accelerating voltage of 120 kV. The BET surface area measurement was made by nitrogen absorption employing a Micromeritics ASAP 2010 instrument and then calculated using the five point BET theory. A Perkin-Elmer CHN elemental analyzer (Model: 2400(II)) was employed to measure the content of residual carbon. The magnetic measurements were performed on a vibrating sample magnetometer (VSM; Toei, VSM-5) at room temperature in an operating range of ± 15 kOe.

3. Results and discussion

3.1. Thermodynamic analysis

To understand the variation of adiabatic flame temperature (T_{ad}) with respect to the OB value, the following equation is used to calculate theoretically the adiabatic T_{ad} for a combustion reaction [6]:

$$T_{ad} = T_0 + \frac{\Delta H_r - \Delta H_p}{c_p}, \quad (3)$$

where T_0 is 25 °C, ΔH_r and ΔH_p are the enthalpies of formation of the reactants and products, respectively, and c_p is the heat capacity of the products at constant pressure. Substituting the thermodynamic data from Table 1 [9,17], Eqs. (1), and (2) into Eq. (3), the variations of T_{ad} together with the amount of gas produced versus the OB value are shown in Fig. 2. As can be seen, the theoretical T_{ad} decreases substantially with increasing OB value of the reactant mixture, whereas the amount of produced gas is slightly decreased with the increase of OB value up till OB = 0 and begins to rapidly increase with further increase in OB value.

3.2. Nature of combustion reaction

In this work, it was found that the nature of the combustion reaction and the characteristics of as-synthesized product are dependent on the OB value. Typical temperature histories of the reactant mixtures with OB= 0, −8% and +5% during combustion reaction are shown in Fig. 3. When OB = 0 was used, once the reactant mixture was ignited, the temperature increased suddenly up to a maximum of ~1250 °C and then began to decrease (The maximum temperature during combustion reaction is symbolized as T_c). In the case of OB = +5%, T_c is 995 °C. In addition, a shoulder of round shape is observed in the temperature profile between 240 and 280 °C, which could be caused by the endothermic decomposition of NH_4NO_3. When using OB = −8%, the temperature increased slowly and, after a period of time, it reached to a maximum of ~700 °C and then began to decrease. It is interesting to notice that the slope of the temperature versus time curve for OB = 0 is more abrupt than those of the other two cases, signifying that its reaction rate is more rapid.

The plot of T_c as a function of OB value together with its regimes having characteristic reaction is also shown in Fig. 2. T_c is typically lower than the calculated value of T_{ad} due to heat loss [18] and/or incomplete reaction. In addition, T_c increases with increasing OB value by reaching to a maximum of ~1300 °C (at OB = −2%) and then decreases with further increment in OB value.

Table 1
Entropy of formation and specific heat for the combustion synthesis of Ni–Zn ferrite

Compound	ΔH_f° (kJ/mol)	c_p (kJ/mol K)	Notes
$Ni(NO_3)_{2(c)}$	−428		
$Zn(NO_3)_{2(c)}$	−482		OB = −96%, Heat of combustion = −973 kJ/mol
$Fe(NO_3)_{3(aq)}$[a]	−671		OB = +20%, Heat of combustion = −210 kJ/mol
$NH_2CH_2COOH_{(c)}$	−528		
$NH_4NO_{3(c)}$	−365		
$Ni_{0.5}Zn_{0.5}Fe_2O_{4(c)}$[b]	−1041	0.148	
$CO_{2(g)}$	−395	0.061	
$H_2O_{(g)}$	−243	0.051	
$N_{2(g)}$		0.024	
$O_{2(g)}$		0.039	

[a]The enthalpy of formation of $Fe(NO_3)_{3(aq)}$ was used because that of $Fe(NO_3)_{3\ (c)}$ was not available.

[b]Due to a lack of thermodynamic data for $Ni_{0.5}Zn_{0.5}Fe_2O_4$, the average enthalpy and specific heat of $Fe_3O_{4(c)}$ ($\Delta H_f^0 = -1117$ kJ/mol, $c_p = 0.147$ kJ/mol K) and $CuFe_2O_{4(c)}$ ($\Delta H_f^0 = -965$ kJ/mol, $c_p = 0.149$ kJ/mol K) were used [9] because these compounds are isostructure and these divalence metallic radii (Fe^{2+}, Ni^{2+}, Cu^{2+}, and Zn^{2+}) are nearly the same [19].

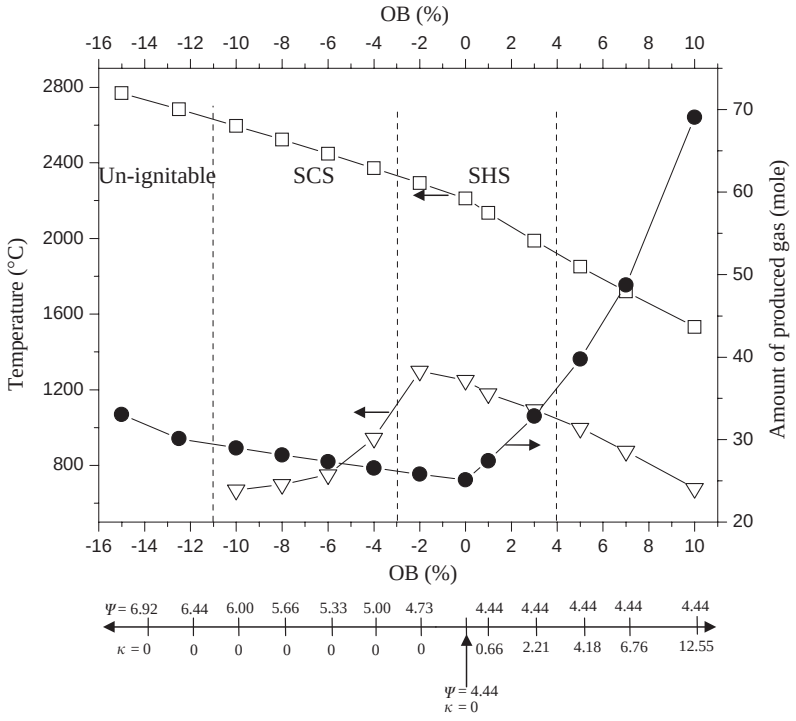

Fig. 2. Theoretical adiabatic flame temperature (T_{ad}) and amount of produced gas, and maximum combustion temperature (T_c) achieved for different reaction nature as a function of OB value. (□) T_{ad}, (▽) T_c, and (●) amount of produced gas (SCS = smoldering combustion synthesis; SHS = self-propagating high-temperature synthesis).

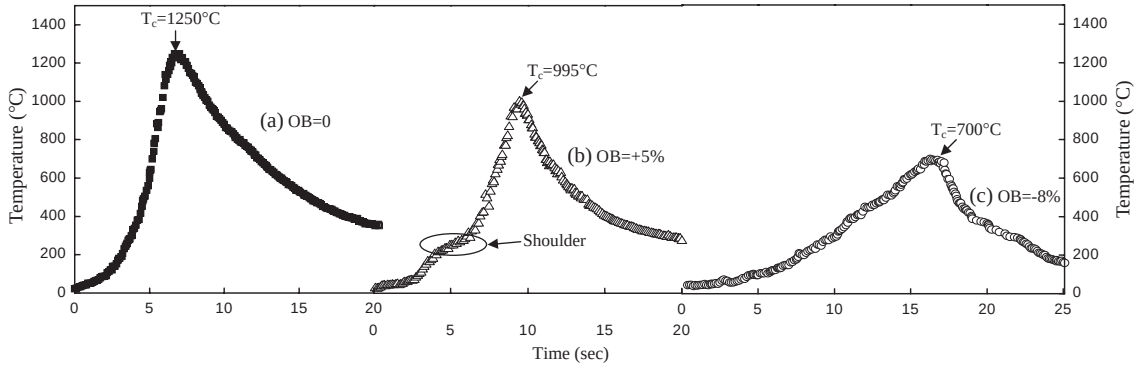

Fig. 3. Typical temperature–time histories during combustion for dried reactant mixtures with (a) OB = 0, (b) OB = +5%, and (c) OB = −8%.

Depending on the OB value, the reaction may be classified into three different modes from our observation:

1. Un-ignitable $OB < -10\%$.
2. Smoldering Combustion Synthesis (SCS), when $-10\% \leqslant OB < -3\%$, $T_c < 950\,^{\circ}C$, and when $OB > +4\%$, $T_c < 1000\,^{\circ}C$;
3. Self-propagating High-temperature Synthesis (SHS), $-3\% < OB < +4\%$, $1100\,^{\circ}C < T_c < 1300\,^{\circ}C$.

SCS mode is characterized by a slow, essentially flameless reaction. When there is an excess fuel ($-10\% \leqslant OB < -3\%$), the combustion reaction needs oxygen to be supplied externally. Oxygen enters via diffusion action into the reaction zone controlled by kinetic factors that limit the reaction rate and, eventually, the SCS reaction mode. In an extreme case ($OB < -10\%$), the combustion reaction may not be ignited. The characteristic feature of the SHS mode is that the reaction initiates locally and it propagates as a combustion wave in a self-sustained manner through the reaction volume. In this regime, it is to be emphasized that the fuel-to-oxidant ratio is within a proper range ($-3\% < OB < +4\%$) and the oxygen content contained in the reactant mixture is the main source of oxygen

required for combustion reaction. Meanwhile, oxygen can react with glycine and oxidize/consume most of the fuel as it originates from NO_3^-, thus resulting in the phenomenon of SHS reaction. With increased OB value ($> +4\%$), since the fuel content is small, the heat evolved is not enough and thus the temperature is lower. This leads to slower reaction rates as manifested in the smoldering combustion behavior.

3.3. Characterization of as-synthesized powders

In the following experiments, the OB values of -8%, 0 and $+5\%$ were selected to represent fuel-rich, stoichiometric and fuel-lean compositions, respectively. Fig. 4 shows the XRD patterns of the as-synthesized powders prepared at the three different OB values. The characteristic peaks of spinel phase were observed for all cases. When OB $= -8\%$ was used, the XRD pattern of the as-synthesized product is different from the other two cases due to its relatively low signal/noise ratio. In addition, the diffraction peaks of Fe_2O_3 and some unknown peaks were also observed, which delineates that the as-synthesized powder consists of impurities.

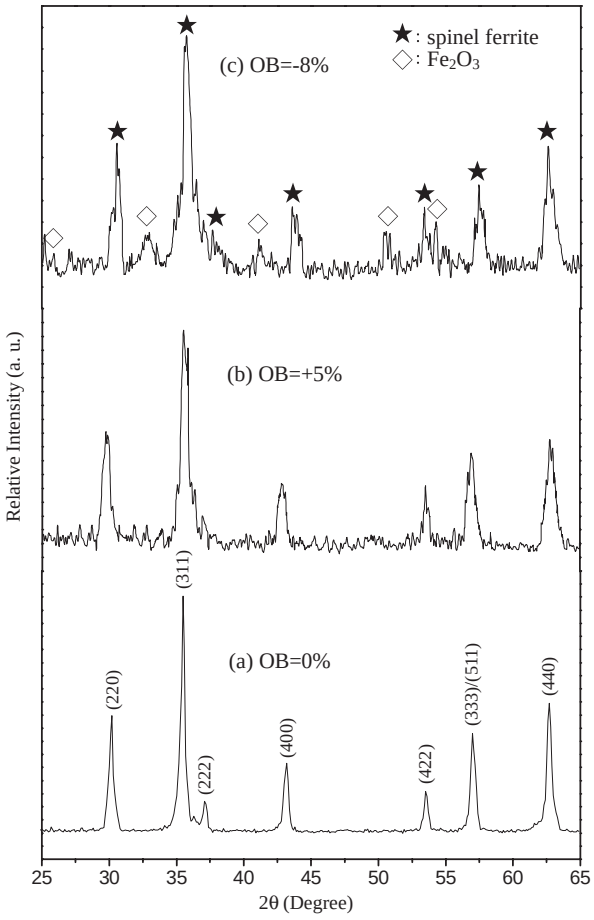

Fig. 4. XRD patterns of as-synthesized product made with (a) OB = 0, (b) OB = +5%, and (c) OB = −8%.

There exists a notably broadening phenomenon in terms of diffraction peaks of the products prepared using OB $= -8\%$ and $+5\%$, which may be attributed to the fact that the products' crystallite are relatively fine.

The lattice constant a was determined by using the classical formula:

$$a = \frac{\lambda}{2}\frac{[h^2 + k^2 + l^2]^{1/2}}{\sin\theta}, \quad (4)$$

where λ is the wavelength of Cu$K\alpha$, (hkl) are the Miller indices, and θ is the diffraction angle corresponding to the (hkl) plane. The a values of the as-synthesized ferrites are 8.3453, 8.3782, and 8.4130 Å for OB $= -8\%$, 0 and $+5\%$, respectively. Though these values are different from the value of $a = 8.38$ Å for $Ni_{0.5}Zn_{0.5}Fe_2O_4$ in Ref. [20]. All of them fall in between the lattice constant ($a = 8.3393$ Å) of $NiFe_2O_4$ [21] and the lattice constant ($a = 8.4411$ Å) of $ZnFe_2O_4$ [22]. Judging from the Ref. [23], it can be inferred that the spinel phase is Ni–Zn ferrites.

Table 2 presents the characteristics of the as-synthesized powder prepared at the three different OB values. The grain size of the as-synthesized products was

Table 2
Effect of OB value on characteristics of as-synthesized powders

OB (%)	Crystallite size[a] (nm)	Surface area (m^2/g)	Carbon content (wt%)
−8 (fuel-rich)	27.8	39.1	9.25
0 (stoichiometric)	34.5	30.2	1.53
+5 (fuel-lean)	25.3	44.5	2.15

[a]Crystallite size of the as-synthesized $Ni_{0.5}Zn_{0.5}Fe_2O_4$ powders calculated from the line broadening of the (311) XRD peak by Scherrer formula.

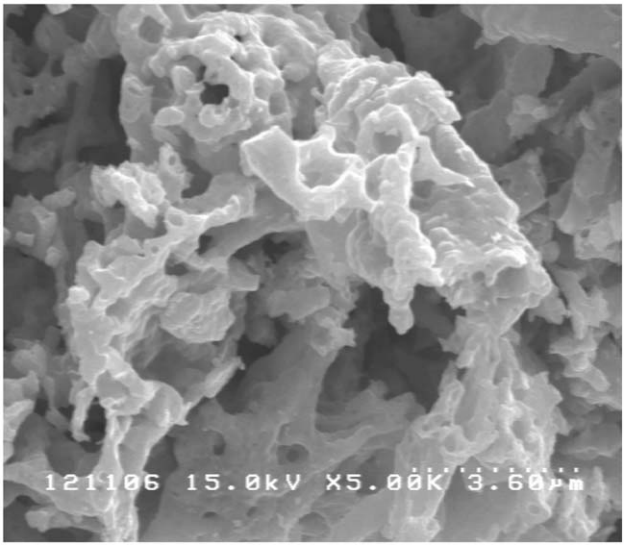

Fig. 5. Typical SEM micrograph of as-synthesized product made with $OB = 0$.

estimated according to the Scherrer formula [24]. It was found that all the products obtained in this work are nanocrystallites with the sizes ranging between 25 and 35 nm, which are smaller than the critical size of mono-magnetic-domain (40 nm for Ni–Zn ferrite [25]) and thus these as-synthesized samples may display a superpar-amagneic behavior. Also, their surface areas are large ($\sim$30–45 m^2/g), and the as-synthesized powder obtained using OB = +5% has the largest specific surface area as compared with that of using OB = 0 and −8%. As more gases are evolved during combustion, the reaction heat could be carried away from the system by convection to hinder grain growth, which may produce powder with a high specific surface area. The carbon contents of the as-synthesized product with OB = −8% is relatively high as compared with that of using OB = 0 and +5%. This result coupled with its XRD spectrum with impurity contained (Fig. 2(a)) is attributed to the lesser amount of oxygen available for combustion. Hence, the local temperature of reaction zone remains low ($\sim$700 °C), causing combustion reaction to be incomplete.

Fig. 5 shows the typical SEM photograph of the as-synthesized product prepared with OB = 0. A continuous network of powders is formed. Voids and holes can be seen, which result from the escaping of gases during combustion. By SEM observation, it was found that as the OB value was increased, the porosity of the resultant powders also increased due to the evolution of more-produced amounts of gas. The morphology of as-synthesized powder prepared by using OB = 0 and +5% with their corresponding electron diffraction patterns are shown in Fig. 6. The size of crystallites

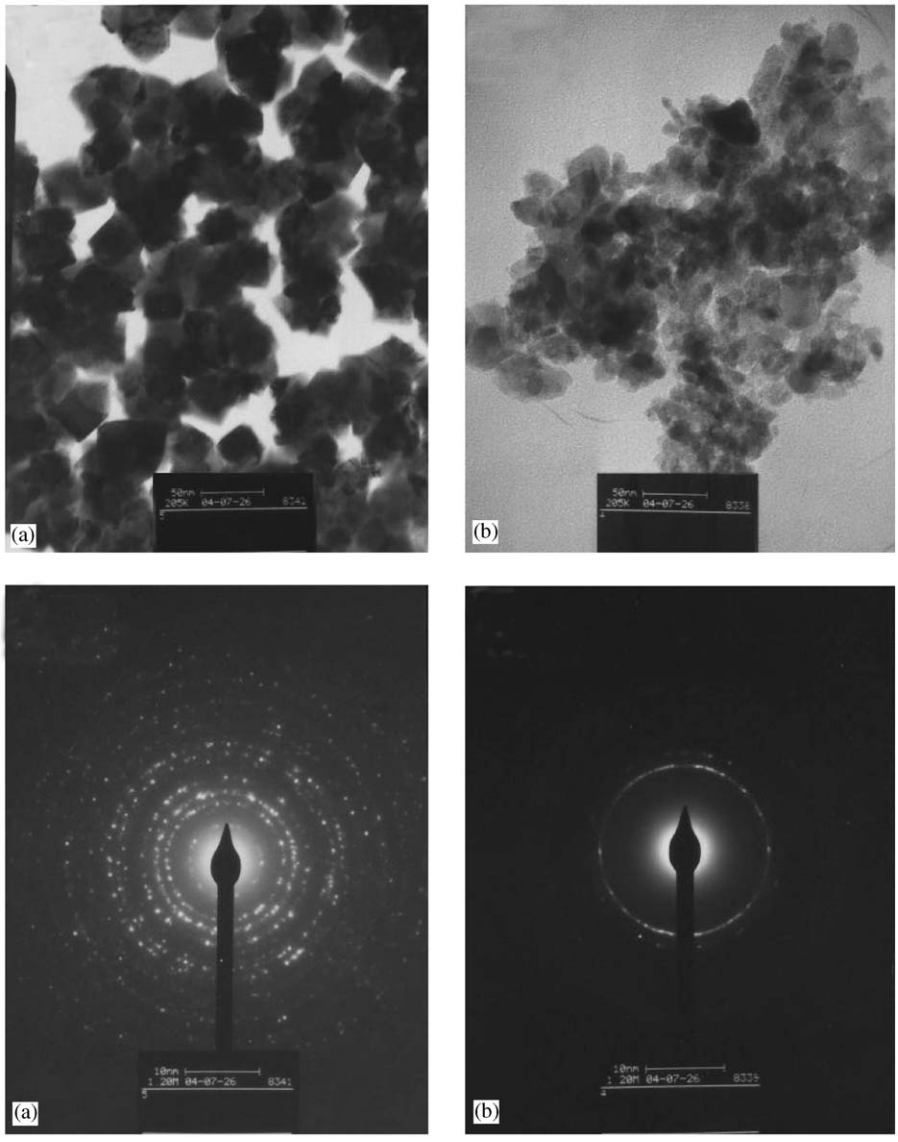

Fig. 6. TEM images of as-synthesized powders with corresponding diffraction patterns for (a) OB = 0 and (b) OB = +5% (Taken under the same operation conditions for both specimens).

were estimated to be ~20–25 nm for the OB = +5% product and ~35–40 nm for OB = 0 one, in terms of which they are about the same sizes as the ones estimated by using XRD method. In addition, diffraction patterns indicate that the OB = 0 product has a higher degree of crystallinity than do the OB = +5% one. (The TEM photograph of the as-synthesized product with OB = −8% is similar to the one using OB = +5%, but not shown here).

Fig. 7 shows the real trace of the hysteresis loops of the as-synthesized powders (crystallite size: <40 nm) and the sintered sample (grain size: ~1.2 μm). The hysteresis loops of the as-synthesized ferrites were characterized to have quite low magnetization values and they do not reach saturation value even at 15 kOe, indicating their superparamagnetic nature. However, on sintering the ferrite at 950 °C/2 h, saturation magnetization was attained (~72 emu/g) at 2.5 kOe. This result is obviously caused by the dependence of grain size on M_s, which can be explained through the transition from mono- to multi-magnetic-domain behavior [25]. As shown in Figs. 7(b) and (c), the maximum magnetization attained for powders synthesized with different OB value was in the order of OB = 0 > OB = +5% > OB = −8%, whereas the order of coercive force was just opposite. It is suggested that impurity content or poor crystallization may affect the magnetic behavior of the as-synthesized ferrite by reducing the maximum magnetization and increasing the coercive force. (It is worth noting that the soft-magnetic properties of the sintered sample are comparable with those obtained by other methods [26–28].) The detailed insights of the reaction mechanism (by means of thermal analysis technique) and the as-synthesized powders' characteristics (such as sinterability, electromagnetic properties), however, require further investigation, which is currently being undertaken.

4. Conclusions

1. A combustion synthesis method has been used to prepare nanocrystalline $Ni_{0.5}Zn_{0.5}Fe_2O_4$ containing a considerably large surface area. Utilization of glycine, metal (Ni, Zn, and Fe) nitrates, ammonium nitrate joined with mixing the reactants without adding water and combining a step of thorough dehydration are the key techniques of this method. Once ignited in air at room temperature, the reactant mixtures undergo a combustion process and directly transform into porous ferrite powders.
2. The combustion reaction is between nitrates and glycine, in that NO_3^- is oxidant and the organic group is fuel. The reaction mode and the combustion temperature can be controlled by changing the oxygen balance (OB) values of the reactant mixtures. Thus, the properties (such as crystallite size, surface area, carbon content, etc.) of as-synthesized product can vary based on OB value.
3. The maximum magnetization and coercive force of the resulting ferrites show a strong dependence on OB value. In addition, the as-synthesized powders

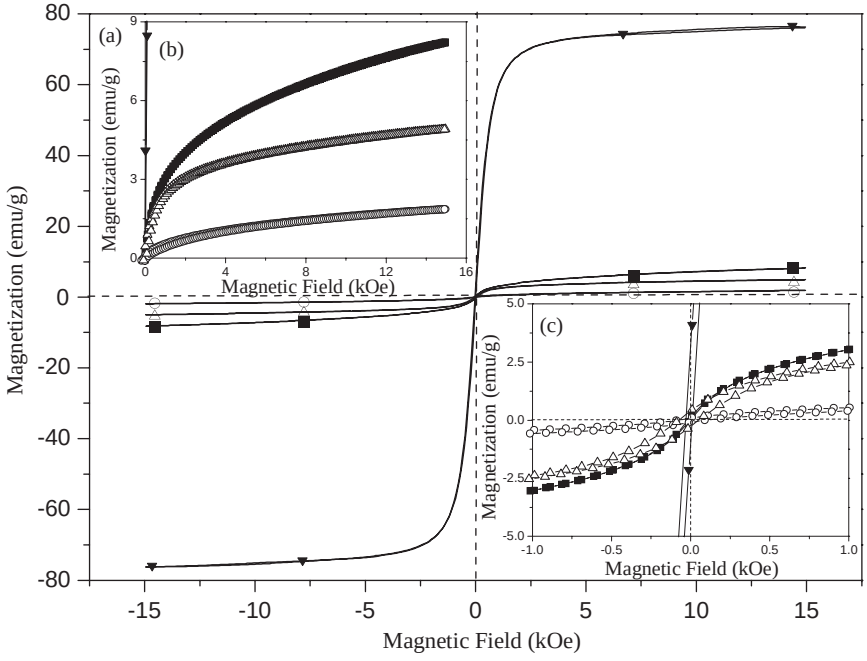

Fig. 7. (a) Room temperature hysteresis loops of as-synthesized powders made with various OB values and the sintered sample obtained by using the product of OB = 0. (b) A zoom plot showing the first quadrant of Fig. 7(a). (c) A zoom plot showing the vicinity of the origin in Fig. 7(a). (■) as-synthesized powder for OB = 0, (△) as-synthesized powder for OB = +5%, (○) as-synthesized powder for OB = −8%, and (▼) sintered sample.

contain a superparamagnetic nature due to their low-ranking and unsaturated magnetization value as compared with those of sintered sample.

Acknowledgment

Support for this research by the National Science Council of the Republic of China under Grant No. NSC 93-2214-E-014-001 is gratefully acknowledged.

References

[1] L.A. Chick, L.R. Pederson, G.D. Maupin, J.L. Bates, L.E. Thomas, G.J. Exarhos, Mater. Lett. 10 (1990) 6–12.
[2] K. Suresh, K.C. Patil, J. Solid State Chem. 99 (1992) 12–17.
[3] J.J. Kingsley, L.R. Pederson, Mater. Res. Soc. Symp. Proc. 296 (1993) 361–366.
[4] L.E. Shea, J. McKittrick, O.A. Lopez, E. Sluzky, J. Am. Ceram. Soc. 79 (1996) 3257–3265.
[5] C.H. Yan, Z.G. Xu, F.X. Cheng, Z.M. Wang, L.D. Sun, C.S. Liao, J.T. Jia, Solid State Commun. 111 (1999) 287–291.
[6] R.D. Purohit, B.P. Sharma, K.T. Pillai, A.K. Tyagi, Mater. Res. Bull. 36 (2001) 2711–2721.
[7] Y.P. Fu, C.H. Lin, J. Magn. Magn. Mater. 251 (2002) 74–79.
[8] R. Kalai Selvan, C.O. Augustin, L. John Berchmans, R. Saraswathi, Mater. Res. Bull. 38 (2003) 41–54.
[9] R.V. Mangalaraja, S. Ananthakmar, P. Manohar, F.D. Gnanam, M. Awano, Mater. Sci. Eng. A 367 (2004) 301–305.
[10] T.Y. Tsay, K.S. Liu, I.N. Lin, J. Magn. Magn. Mater. 209 (2000) 189–192.
[11] P.S.A. Kumar, J.J. Shrotri, S.D. Kulkarni, C.E. Deshpande, S.K. Date, Mater. Lett. 27 (1996) 293–296.
[12] P.W. Cooper, S.R. Kurowski, Technology of Explosives, Wiley, New York, NY, 1996 (pp. 5–7).
[13] C. Caizer, Mater. Sci. Eng. B 100 (2003) 63–68.
[14] A.F.C.M. Costa, A.P.A. Diniz, L. Gama, M.R. Morelli, R.H.G.A. Kiminami, J. Metastable Nanocryst. Mater. 20–21 (2003) 582–587.
[15] C.C. Hwang, C.Y. Wu, J. Wan, J.S. Tsai, Mater. Sci. Eng. B 111 (2004) 49–56.
[16] R.V. Mangalaraja, S. Ananthakmar, P. Manohar, F.D. Gnanam, M. Awano, Mater. Lett. 58 (2004) 1593–1596.
[17] J.A. Dean, in: Lange's Handbook of Chemistry, 15th ed, McGraw-Hill, New York, 1998.
[18] Z.A. Munir, Am. Ceram. Soc. Bull. 67 (1988) 342–349.
[19] Y.M. Chiang, D.P. Brinie III, W.D. Kingery, Physical Ceramics: Principles for Ceramic Science and Engineering, Wiley, New York, NY, 1997, p. 16.
[20] P.C. Fannin, S.W. Charles, J.L. Dormann, J. Magn. Magn. Mater. 201 (1999) 98–101.
[21] Joint Committee on Powder Diffraction Standards (JCPDS) file number: 44-1485.
[22] Joint Committee on Powder Diffraction Standards (JCPDS) file number: 22-1012.
[23] E.E. Sielo, R. Rotelo, S.E. Jacobo, Physica B 320 (2002) 257–260.
[24] H.P. Klug, L.E. Alexander, X-ray Diffraction Procedures for Polycrystalline and Amorphous Materials, Wiley, New York, 1997 (p. 637).
[25] A.S. Albuquerque, J.D. Ardisson, W.A.A. Macedo, J. Appl. Phys. 87 (2000) 4352–4357.
[26] Y. Hayashi, T. Kimura, T. Yamaguchi, J. Mater. Sci. 21 (1986) 2876–2880.
[27] P.S.A. Kumar, J.J. Shrotri, C.E. Deshpande, S.K. Date, J. Appl. Phys. 81 (1997) 4788–4790.
[28] Y. Li, J. Zhao, J. Han, Mater. Res. Bull. 37 (2002) 583–592.